

# Reduction of $\text{Sr}_2\text{MnO}_4$ Investigated by High Temperature in Situ Neutron Powder Diffraction under Hydrogen Flow

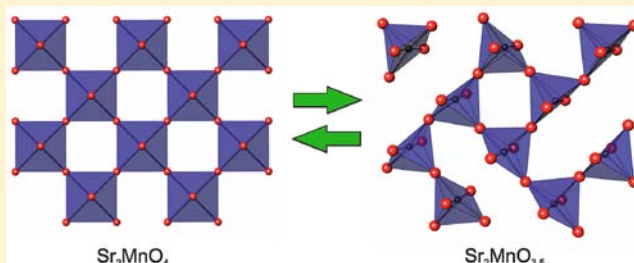
Thibault Broux,<sup>†</sup> Mona Bahout,<sup>\*,†</sup> Olivier Hernandez,<sup>†</sup> Florent Tonus,<sup>†</sup> Serge Paofai,<sup>†</sup> Thomas Hansen,<sup>‡</sup> and Colin Greaves<sup>\*,§</sup>

<sup>†</sup>Institut des Sciences Chimiques de Rennes, UMR CNRS 6226, Université de Rennes 1, 263, Avenue du Général Leclerc, 35042 Rennes, France

<sup>‡</sup>Institut Laue-Langevin, 6, rue Jules Horowitz, 38042 Grenoble Cedex, France

<sup>§</sup>School of Chemistry, University of Birmingham, Edgbaston, Birmingham, B15 2TT, U.K.

**ABSTRACT:** This experiment emphasizes the first example of two-phase sequential Rietveld refinements throughout a solid/gas chemical reaction monitored by Neutron Powder Diffraction (NPD) at high temperature. The reduction of the  $n = 1$  Ruddlesden–Popper (RP) oxide  $\text{Sr}_2\text{MnO}_4$  heated under a flow of 5%  $\text{H}_2$ –He has been investigated throughout two heating/cooling cycles involving isothermal heating at 500 and 550 °C. Oxygen loss proceeds above  $T \sim 470$  °C and increases with temperature and time. When the oxygen deintercalated from the “ $\text{MnO}_2$ ” equatorial layers of the structure results in the  $\text{Sr}_2\text{MnO}_{3.69(2)}$  composition, the RP phase undergoes a first order  $I4/mmm \rightarrow P2_1/c$ , tetragonal to monoclinic phase transition as observed from time-resolved in situ NPD. The phase transition proceeds at 500 °C but is incomplete; the weight ratio of the  $P2_1/c$  phase reaches  $\sim 41\%$  after 130 min of isothermal heating. The fraction of the monoclinic phase increases with increasing temperature and the phase transition is complete after 80 min of isothermal heating at 550 °C. The composition of the reduced material refined to  $\text{Sr}_2\text{MnO}_{3.55(1)}$  and does not vary on extended heating at 550 °C and subsequent cooling to room temperature (RT). The symmetry of  $\text{Sr}_2\text{MnO}_{3.55(1)}$  is monoclinic at 550 °C and therefore consistent with the RT structure determined previously for the  $\text{Sr}_2\text{MnO}_{3.64}$  composition obtained from ex situ reduction. Consequently, the stresses due to phase changes on heating/cooling in reducing atmosphere may be minimized. The rate constants for the reduction of  $\text{Sr}_2\text{MnO}_{4.00}$  determined from the evolution of weight ratio of the tetragonal and monoclinic phase in the time-resolved isothermal NPD data collected on the isotherms at 500 and 550 °C are  $k_{500} = 0.110 \times 10^{-2}$  and  $k_{550} = 0.516 \times 10^{-2} \text{ min}^{-1}$  giving an activation energy of  $\sim 163 \text{ kJ mol}^{-1}$  for the oxygen deintercalation reaction.



## 1. INTRODUCTION

Manganese oxides<sup>1–4</sup> have been the focus of much attention owing to their tendency to display colossal magnetoresistance (CMR) and hence their potential as magnetic sensors or reading heads in magnetic storage devices. In addition, strontium substituted lanthanum perovskite manganates  $\text{La}_{1-x}\text{Sr}_x\text{MnO}_{3-\delta}$  (LSM) are well established cathode materials for high temperature solid oxide fuel cells (SOFC).<sup>5</sup> Recent trends in SOFC research have targeted the development of new materials for cell components for intermediate-temperature (IT) operation because of performance and longevity issues of cell components associated with high-temperature operation close to 1000 °C. Indeed, the conventional cathode materials (LSM) and  $\text{La}_{1-x}\text{Sr}_x\text{Co}_{1-y}\text{Fe}_y\text{O}_{3-\delta}$  (LSCF) suffer mechanical cracking (a result of thermal expansion mismatching) and unwanted formation of insulating phases at high temperature operating conditions. Recent studies have shown that the Ruddlesden–Popper (RP) class of materials described by the general formula  $A_{n+1}B_n\text{O}_{3n+1}$  ( $A$  = lanthanide or alkaline-earth metal,  $B$  = transition metal), may offer viable alternatives<sup>6,7</sup> as cathode materials for IT-SOFC. The majority of investigations

have concentrated on the suitability of Ni, Co, Cu and Fe RP oxides with  $n = 1$  (so-called  $\text{K}_2\text{NiF}_4$ -type)<sup>8–10</sup> as cathodes for SOFC operating at temperatures below 700 °C and showed that  $\text{La}_2\text{NiO}_4$ -based phases are the most promising.<sup>8,11,12</sup> Conversely, little work has been reported on the closely related Manganite phases.<sup>13,14</sup> Benabad et al. explored the dimensionality of the magnetic interactions in  $\text{Sr}_{1+x}\text{La}_{1-x}\text{MnO}_4$  ( $0 \leq x \leq 1$ ) and reported that annealing the compositions with high  $\text{Mn}^{4+}$  content should be carried out in air at 1400–1450 °C.<sup>15</sup> Munnings et al.<sup>13</sup> prepared  $\text{La}_{2-x}\text{Sr}_x\text{MnO}_{4\pm\delta}$  ( $0.6 \leq x \leq 2.0$ ) solid solutions by a solid state route, with annealing carried out in argon or in 5%  $\text{H}_2$  atmosphere, and investigated the electrical conductivity and high temperature stability in air by in situ high temperature X-ray diffraction. Sun et al.<sup>14</sup> studied the  $\text{Sr}_{2-x}\text{La}_x\text{MnO}_{4+\delta}$  ( $x = 0.4, 0.5, 0.6$ ) compositions in view of SOFC cathode applications and found that the  $x = 0.6$  phase exhibits the maximum electrical conductivity value ( $5.7 \text{ S cm}^{-1}$

Received: October 16, 2012

Published: January 7, 2013

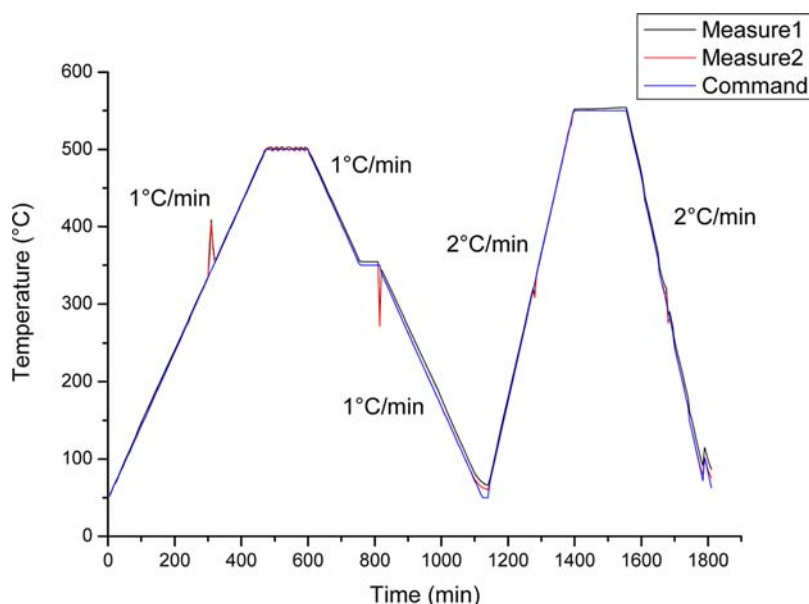


**Figure 1.** Heating and cooling cycles under 5% H<sub>2</sub>–He flow carried out on Sr<sub>2</sub>MnO<sub>4</sub> in the in situ NPD experiment. The temperature overflow at  $T \sim 350$  °C is due to change in the furnace heating mode.

at 800 °C in air) and the lowest cathode overpotential, although this material does not meet other requirements.

The stoichiometric Sr<sub>2</sub>MnO<sub>4</sub> material has been extensively studied, the interest being directed to the determination of the structural chemistry and bidimensional magnetic properties.<sup>16–18</sup> Sr<sub>2</sub>MnO<sub>4– $\delta$</sub>  has been shown to undergo phase transformations as the oxygen content varies, thus altering the Mn valence and hence the Mn–O bond lengths.<sup>19</sup> It was initially reported that the oxygen deficient materials Sr<sub>2</sub>MnO<sub>4– $\delta$</sub>  adopted the tetragonal  $I4/mmm$  space group with a statistical distribution of the vacancies within the “MnO<sub>2</sub>” layers.<sup>20,21</sup> More recently, Gillie et al.<sup>19</sup> refined the structure of Sr<sub>2</sub>MnO<sub>3.64</sub> at room temperature (RT) in the monoclinic space-group  $P2_1/c$  from ex situ RT Neutron Powder Diffraction (NPD). The oxygen vacancies form an original ordered arrangement within the perovskite blocks consisting of corner-sharing MnO<sub>5</sub> square-based pyramids different from those observed for the defect perovskites SrMnO<sub>2.5</sub> and CaMnO<sub>2.5</sub>. Thermo-Gravimetric Analysis (TGA) indicated that the pure Mn<sup>3+</sup> composition Sr<sub>2</sub>MnO<sub>3.50</sub> can be obtained under dilute hydrogen at 550 °C. In this regard, we investigated in this contribution the reduction of Sr<sub>2</sub>MnO<sub>4– $\delta$</sub>  under a flow of 5% H<sub>2</sub>–He using in situ NPD. Our intention was to determine the temperature at which oxygen loss occurs, improve the knowledge of the phase transition, and examine the structural relationship in the composition range Sr<sub>2</sub>MnO<sub>3.50</sub>–Sr<sub>2</sub>MnO<sub>3.64</sub>. Moreover, this experiment allows us to check if the monoclinic structure established for Sr<sub>2</sub>MnO<sub>3.64</sub> at RT in air<sup>19</sup> is retained at high temperature under hydrogen flow (i.e., under SOFC operating conditions) and if the cooling rate can affect the vacancy pattern with respect to the various possibilities for linking MnO<sub>5</sub> square pyramids.<sup>22,23</sup> It is worthwhile mentioning that no high temperature structural characterization has been carried out on manganites under hydrogen flow despite possible applications as anode materials for SOFCs. In fact many compositions withstand reducing conditions and exhibit higher thermal stability than perovskites with similar transition-metal ions.<sup>24,25</sup> The availability of mixed-valence states Mn(II/III)<sup>26</sup> and the flexibility of manganese to various coordination

environments<sup>19,22,23,26–29</sup> facilitating oxygen ion diffusion through anion-vacancy pathways might confer Mixed Ionic Electronic Conducting (MIEC) properties to such layered manganites.

## 2. EXPERIMENTAL SECTION

**2.1. Synthesis.** A powder sample with nominal composition Sr<sub>2</sub>MnO<sub>4</sub> was prepared via the citrate/ethylene glycol sol–gel route. MnO (Aldrich, 99%) and SrCO<sub>3</sub> (Aldrich,  $\geq 99.9\%$ ) were dissolved in dilute nitric acid warmed to 80 °C. An excess of SrCO<sub>3</sub> (2 mol %) was required to obtain a single-phase sample, presumably because of a degree of volatilization. Citric acid (Acros Organic, 99%) and ethylene-glycol (Sigma-Aldrich, > 99%) were added to the solution to give an ethylene-glycol: citric-acid: metal ion molar ratio of 4:2:1. The mixture was then stirred and heated until a gel and subsequently a resin formed. The resin was calcined at  $\sim 600$  °C in air overnight to decompose the organic components. This precursor was then ground and pressed into pellets (2 mm thickness, 13 mm diameter) which were heated in air at 1550 °C for 24 h with one intermediate grinding and cooled at  $\sim 4$  °C min<sup>–1</sup>.

**2.2. Preliminary Analysis of the Product.** The reaction product was characterized by X-ray powder diffraction (XRD) using a Bruker AXS D8 Advance diffractometer equipped with a Germanium primary monochromator (selecting  $K\alpha_1$  radiation) and a Lynxeye detector. Thermogravimetric analysis (TGA) was performed on a Setaram TG 92 thermal analyzer. A powder sample of  $\sim 50$  mg was loaded in a quartz crucible and heated in 5% H<sub>2</sub>–N<sub>2</sub> flow at a rate of 10 °C min<sup>–1</sup> to 550 °C and held at this temperature for 4 h before quick cooling to RT.

**2.3. Neutron Diffraction.** NPD experiments were carried out on the high-flux two-axis neutron powder diffractometer D20<sup>30</sup> at the Institut Laue Langevin (ILL, Grenoble, France) according to the strategy described previously.<sup>31</sup> A takeoff angle of 118° from the (117) plane of a germanium monochromator was chosen, giving a wavelength of  $\lambda = 1.3594(1)$  Å and a resolution of  $\Delta d/d \sim 1.6 \times 10^{-2}$ , while retaining a high flux on the sample ( $\sim 10^8$  n cm<sup>–2</sup> s<sup>–1</sup>). A sample of  $\sim 3$  g was loaded in the center of a quartz tube (8 mm inner diameter) between two pieces of quartz wool which allowed unrestricted gas flow over the sample, while also acting as the support. Two K-type thermocouples were placed in the quartz tube: one a few mm above the sample to monitor the temperature and another just below the sample to regulate the temperature. The in situ thermal

treatment under hydrogen flow was as follows: the sample was heated to  $\sim 500$  °C at a rate of  $1$  °C  $\text{min}^{-1}$  then held at  $500$  °C for  $\sim 130$  min before cooling to  $RT$  at a rate of  $1$  °C  $\text{min}^{-1}$ . To assess a better reduction level, the sample was subsequently heated to  $\sim 550$  °C at  $2$  °C  $\text{min}^{-1}$  and allowed to equilibrate at  $550$  °C for  $\sim 160$  min before cooling to  $RT$  at  $2$  °C  $\text{min}^{-1}$ . The heating/cooling cycles are displayed in Figure 1.

Diffraction patterns were collected every 5 min throughout the aforementioned heating/cooling ramps giving a maximum temperature resolution of  $5$  °C. In addition, isothermal data were collected at  $\sim 500$  and  $550$  °C, as well as at  $RT$  at the beginning of the experiment and after each reduction cycle. The diffraction patterns were analyzed sequentially by the Rietveld method<sup>32,33</sup> using the FullProf program.<sup>34</sup> The background initially modeled using a 36-parameter Chebyshev polynomial (obtained in JANA)<sup>35</sup> was treated iteratively by Fourier filtering technique. The peak profiles were modeled using a Thompson–Cox–Hastings pseudo-Voigt profile function;<sup>36</sup> two asymmetry parameters were refined below  $2\theta = 55^\circ$ . In the tetragonal symmetry, the  $z$ -coordinates of Sr and the axial oxygen atom (O1) position were refined along with the occupancy factors of the equatorial oxygen (O2) position and the isotropic displacement parameters ( $B_{\text{iso}}$ ) of all the atoms. In the monoclinic symmetry, the  $B_{\text{iso}}$  of the Mn atoms were constrained to be equal. Similarly, the  $B_{\text{iso}}$  of the apical O atoms were constrained equal, as were the equatorial O atoms in the “ $\text{MnO}_2$ ”. To avoid divergence, especially when the monoclinic phase is minor, geometric soft-restraints were applied on Mn–O polyhedra, Sr–Mn, Mn–Mn, and Sr–Sr distances. For a good estimation of the standard deviations on the soft-restraints for the interatomic distances and the angles in the Mn–O coordination polyhedra, the monoclinic phases are compared at high and low temperature. The atomic positions were refined assuming a variation of  $0.01$  Å for the Mn–O bond length,  $0.02$  Å for the Sr–Sr, Sr–Mn, and Mn–Mn bond lengths and  $2^\circ$  for the Mn–O–Mn angle. When the monoclinic phase prevails on the  $550$  °C isotherm and subsequent cooling to  $RT$ , the geometrical soft-restraints are no more used.

### 3. RESULTS

**3.1. Preliminary Analysis.** XRD data collected from the as-prepared  $\text{Sr}_2\text{MnO}_4$  sample indicated the formation of a single

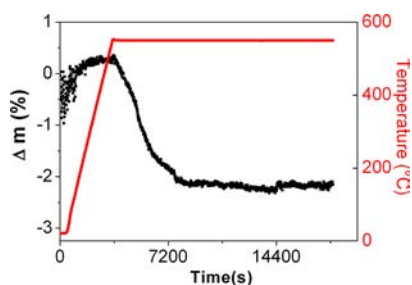


**Figure 2.** TGA of  $\text{Sr}_2\text{MnO}_4$  under 5%  $\text{H}_2$ – $\text{N}_2$  with a heating rate of  $10$  °C  $\text{min}^{-1}$ . The sample was held at  $550$  °C under the gas flow for 4 h before fast cooling to  $RT$ .

**Table 1.**  $RT$  Structure Parameters of As-Prepared  $\text{Sr}_2\text{MnO}_{4.00}$  Obtained from NPD<sup>a</sup>

atom	$x$	$y$	$z$	$B_{\text{iso}}$ (Å <sup>2</sup> )	occupancy
Sr	0	0	0.35577(7)	0.52(2)	1.00
Mn	0	0	0	0.29 (3)	1.00
O1	0	0	0.15605(10)	0.61(3)	1.00
O2	0	0.5	0	0.51(2)	1.00

<sup>a</sup>Space group  $I4/mmm$  (139):  $a = 3.78925(2)$  Å,  $c = 12.4991(1)$  Å,  $V = 179.467(2)$  Å<sup>3</sup>,  $Z = 2$ ,  $R_{\text{wp}} = 7.31\%$ ,  $R_p = 7.31\%$ ,  $R_{\text{Bragg}} = 1.90\%$ , and  $\chi^2 = 4.27$ . The occupation of all atoms were fixed in the final refinement.

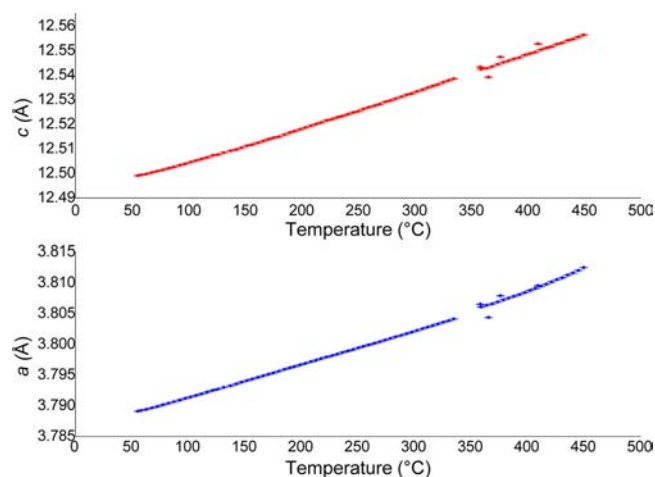


**Figure 3.** Evolution of the lattice parameters of  $\text{Sr}_2\text{MnO}_{4-\delta}$  as a function of temperature along the first heating ramp ( $20$ – $500$  °C) under 5%  $\text{H}_2$ –He flow. The discontinuity at  $T \sim 300$  °C is due to the heat overflow seen in Figure 1.

tetragonal  $n = 1$  RP,  $\text{K}_2\text{NiF}_4$ -like phase (space group  $I4/mmm$ ) with no impurity phases. The results deduced from TGA under a flow of 5%  $\text{H}_2$ –Ar are shown in Figure 2. A mass loss of  $\sim 2\%$  corresponding to 0.37 oxygen per formula unit was observed at  $550$  °C. Given the stoichiometric oxygen-composition of the as-prepared sample, this mass loss corresponds to change from  $\text{Sr}_2\text{MnO}_{4.00}$  to  $\text{Sr}_2\text{MnO}_{3.63(5)}$ . However, because of uncorrected buoyancy effects, this mass loss is underestimated, and the oxygen content in the reduced sample should be lower.

**3.2. Neutron Diffraction.** NPD patterns were collected at  $RT$  on the as-prepared material. From the Rietveld refinement, it was clear that a single phase material had successfully been produced through the Pechini synthesis route. Refinements using the tetragonal  $I4/mmm$  model gave a good fit with  $\chi^2 = 4.24$ ,  $R_{\text{wp}} = 8.36\%$ , and  $R_p = 7.27\%$ . The oxygen occupancies at the axial (O1) and equatorial (O2) sites both refined to 1.02(1) indicating absence of oxygen vacancies and were set to 1.00. The lattice constants  $a = 3.78925(2)$  Å and  $c = 12.4991(1)$  Å, are consistent with those determined by Bouloux et al.<sup>16</sup> from powder X-ray diffraction on the material prepared at  $1650$  °C in air. Details of the NPD refinement are given in Table 1.

This first heating under hydrogen flow was limited to  $500$  °C to avoid decomposition into the metal oxides SrO and MnO as observed in a previous in situ NPD experiment when the sample was heated up to  $600$  °C. Sequential Rietveld refinements along the heating ramp ( $20$ – $500$  °C) using a single tetragonal  $I4/mmm$  phase show that the oxygen occupancy at the axial position (O1) was unchanged within the estimated standard deviations and was therefore fixed to 1.00 whereas a very slight deficiency, corresponding to an occupancy factor of  $\sim 0.96(2)$ , was detected on the equatorial oxygen position (O2) above  $\sim 470$  °C. The linear variation of the lattice parameters displayed in Figure 3 is consistent with the absence of significant oxygen loss or phase transition below  $500$  °C. The thermal expansion coefficients (TECs) for the tetragonal phase correspond to  $14.36 \times 10^{-6} \text{ K}^{-1}$  perpendicular to  $[001]$  and  $12.70 \times 10^{-6} \text{ K}^{-1}$  along  $[001]$ , resulting in an average value of  $13.81 \times 10^{-6} \text{ K}^{-1}$ . These values are consistent with those obtained by Munnings et al. from high-temperature X-ray diffraction experiments in air<sup>13</sup> and reveal good thermo-mechanical compatibility of  $\text{Sr}_2\text{MnO}_4$  as anode with the

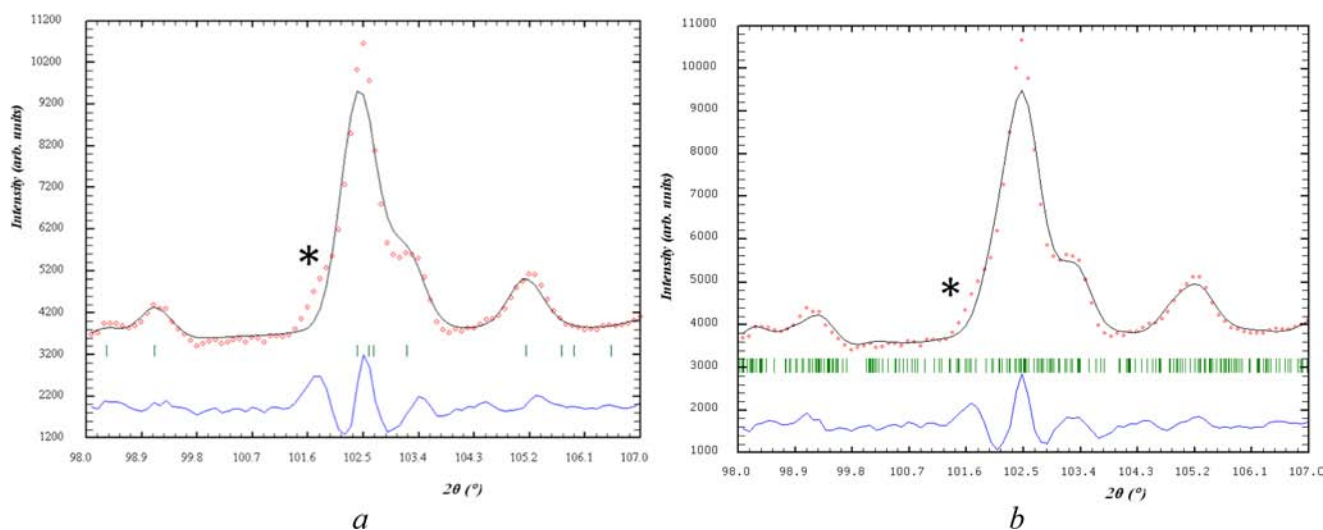


**Figure 4.** Part of the observed and calculated diffraction patterns of  $\text{Sr}_2\text{MnO}_{4-\delta}$  collected for 5 min after extended heating at 500 °C under 5% $\text{H}_2$ –He assuming (a) single-phase  $I4/mmm$  tetragonal or (b) monoclinic models. The peak labeled (\*) is inconsistent with monophasic models but can only be accounted for assuming a biphasic model.

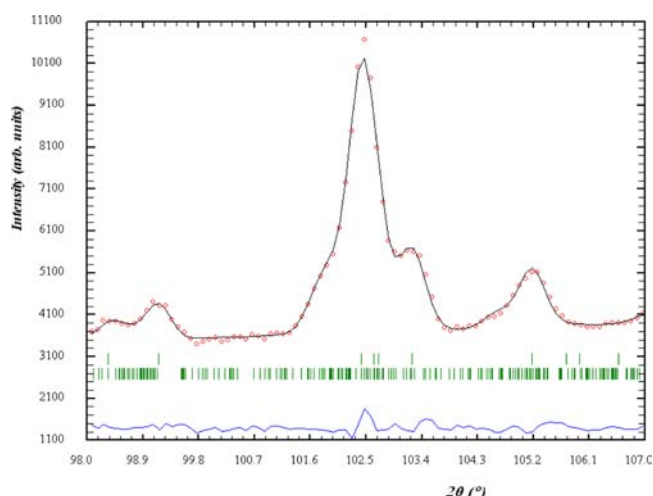


**Figure 5.** Part of the observed and calculated diffraction patterns of  $\text{Sr}_2\text{MnO}_{4-\delta}$  after extended heating (130 min) at 500 °C under 5% $\text{H}_2$ –He. The calculated diffraction pattern derives from a biphasic model consisting of an  $I4/mmm$  tetragonal phase and a  $P2_1/c$  monoclinic phase (upper and lower reflection markers, respectively).

standard SOFC electrolytes. Indeed, electrolyte materials such as yttria-stabilized zirconia (YSZ), lanthanum strontium gallate magnesite (LSGM), and ceria-based compositions have TECs of  $\sim 10$ – $12.5 \times 10^{-6} \text{ K}^{-1}$ .<sup>37,38</sup>

On isothermal heating at 500 °C, a progressive deterioration of the quality of the Rietveld refinements reveals that the space group  $I4/mmm$  was unable to provide acceptable agreement between the observed and the calculated profiles. Indeed, after 50 min, additional peaks inconsistent with the  $I4/mmm$  symmetry of the original phase were clearly visible as illustrated in Figure 4. The intensity and number of these superstructure reflections increased on extended heating clearly, suggestive of a structural transition.

The superstructure peaks cannot be indexed on any decomposition products (MnO or SrO). Since the heated sample is not in thermodynamic equilibrium, the presence of two  $\text{Sr}_2\text{MnO}_{4-\delta}$  phases with variable oxygen content and/or symmetry was assumed. The hypothesis of considering an

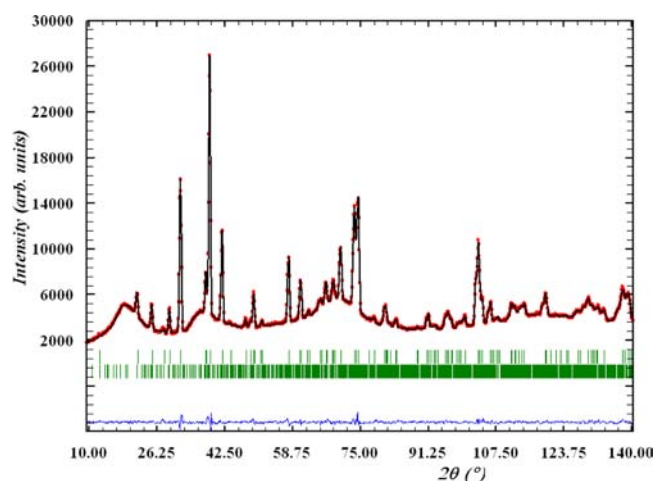


**Figure 6.** Observed and calculated diffraction patterns of  $\text{Sr}_2\text{MnO}_{4-\delta}$  at 60 °C after the first reducing cycle. The calculated diffraction pattern derives from a model consisting in a  $I4/mmm$  tetragonal phase and a  $P2_1/c$  monoclinic phase (upper and lower reflection markers, respectively). A difference profile is also shown.

inhomogeneous composition during a reduction reaction is not unreasonable since the quantity of material used is large ( $\sim 3$  g) to ensure fast exchange of gas throughout the sample and the diffraction data are averaged over relatively long time (5 min). To improve the refinements, a first option was to consider the growth of a second (reduced) tetragonal phase but was quickly discarded after unsuccessful attempts to model it. The second option was based on the defect structure of  $\text{Sr}_2\text{MnO}_{3.5+x}$  refined by Gillie et al.<sup>19</sup> and assumes the existence of an oxygen deficient monoclinic  $P2_1/c$  phase. This hypothesis was consistent with the good fits in the end of the experiment based on a single monoclinic  $P2_1/c$  model. The  $P2_1/c$  space group fits well the superstructure peaks observed at 500 °C such that at  $2\theta \sim 101.4^\circ$  (see Figure 4) which was indexed as  $(3\ 4\ 8)$ ,  $(4\ 8\ 4)$ ,  $(-7\ 4\ 8)$ , and  $(-6\ 8\ 4)$ . Consequently, two-phase sequential Rietveld refinements consisting in an  $I4/mmm$  phase and a  $P2_1/c$  phase were performed for the isothermal data at 500 °C. Because of the lower monoclinic symmetry and

Table 2. Structure Parameters of Sr<sub>2</sub>MnO<sub>4-δ</sub> at 60 °C after the First Reducing Cycle

atom	x	y	z	B <sub>iso</sub> (Å <sup>2</sup> ) <sup>a</sup>	occupancy
<i>I4/mmm</i> phase <sup>b</sup>					
Sr	0	0	0.35489(16)	0.74(4)	1.00
Mn	0	0	0	0.32(4)	1.00
O1	0	0	0.15523(21)	0.66(7)	1.01(1)
O2	0	0.5	0	1.49(6)	0.99(1)
<i>P2<sub>1</sub>/c</i> phase <sup>c</sup>					
Sr1	0.291(3)	0.003(3)	0.072(2)	1.1(4)	1
Sr2	0.292(3)	0.006(3)	0.576(2)	0.7(4)	1
Sr3	0.291(3)	0.246(3)	0.329(2)	1.1(5)	1
Sr4	0.298(3)	0.748(3)	0.319(3)	0.6(4)	1
Mn1	-0.008(2)	-0.002(1)	0.248(1)	0.22(8)*	1
Mn2	-0.010(2)	0.257(1)	0.000(1)	0.22(8)*	1
O1	0.00(1)	0.143(4)	0.130(5)	1.32(9)**	1
O2	0.01(1)	0.115(5)	0.389(6)	1.32(9)**	1
O3	0.00(1)	0.125(7)	0.870(7)	1.32(9)**	1
O4	0.04(1)	0.12(2)	0.63(2)	1.32(9)**	0.38(4)
O5	0.305(3)	0.003(5)	0.336(6)	0.89(7)***	1
O6	0.310(3)	0.012(4)	0.829(6)	0.89(7)***	1
O7	0.307(3)	0.259(7)	0.089(5)	0.89(7)***	1
O8	0.317(3)	0.7420(5)	0.0921(5)	0.89(7)***	1

<sup>a</sup>\*, \*\*, and \*\*\* denote where thermal parameters were constrained to be equal. <sup>b</sup>Space group *I4/mmm*:  $a = 3.80187(5)$  Å,  $c = 12.5223(2)$  Å,  $V = 180.923(5)$  Å<sup>3</sup>,  $Z = 2$ ,  $R_{\text{Bragg}} = 2.73\%$ . <sup>c</sup>Space group *P2<sub>1</sub>/c*:  $a = 6.8444(3)$  Å,  $b = 10.8036(7)$  Å,  $c = 10.7904(9)$  Å,  $\beta = 113.28(1)^\circ$ ,  $V = 732.817(102)$  Å<sup>3</sup>,  $Z = 8$ ,  $R_{\text{Bragg}} = 5.17\%$ ;  $R_p = 8.25\%$ ,  $R_{wp} = 6.85\%$ ,  $\chi^2 = 2.71$ , the weight fraction of the monoclinic phase is  $\sim 41\%$ .

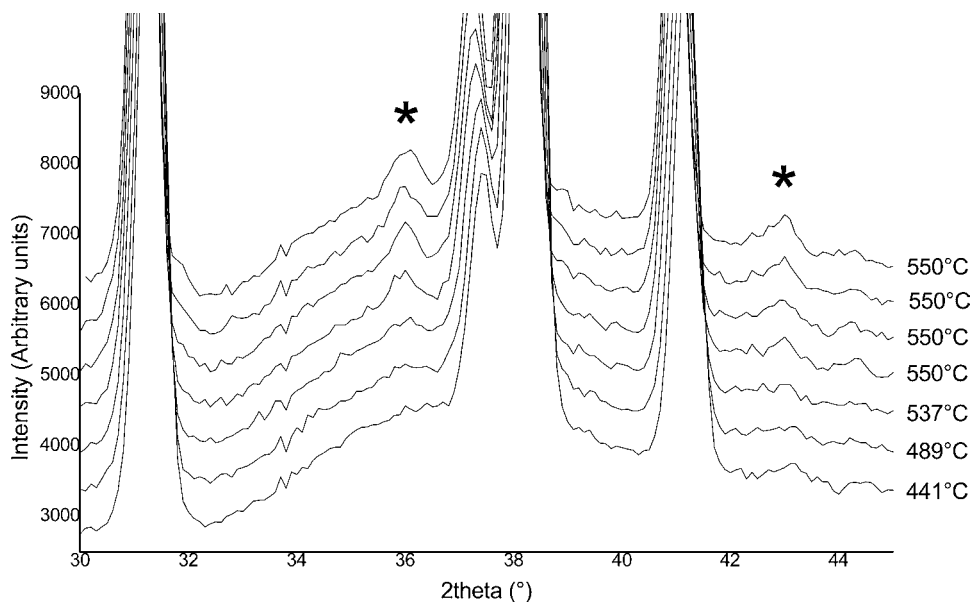
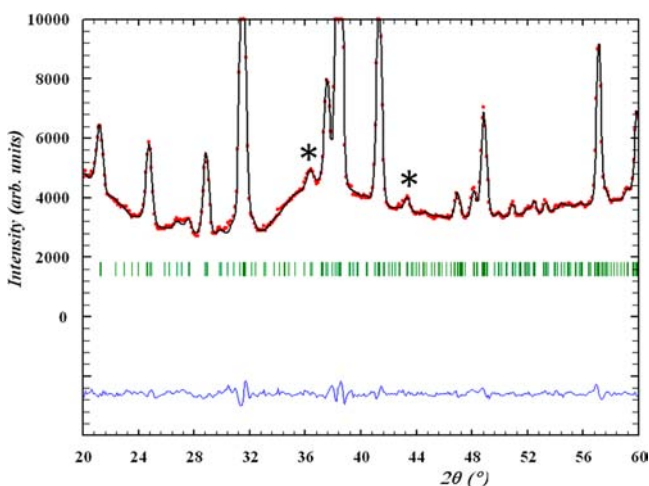


Figure 7. Selected angular range of in situ NPD data on Sr<sub>2</sub>MnO<sub>4-δ</sub> sample heated under 5% H<sub>2</sub>-He flow highlighting the growth of two superstructure peaks labeled (\*) in the *P2<sub>1</sub>/c* space group. Time increases upward for data at 550 °C.

its large unit cell volume, these refinements had to be carried out very carefully. Indeed, the unit cell volume of the monoclinic phase is four times larger than the tetragonal one. The superstructure peaks are weak, especially at the beginning of the isotherm when the fraction of the *P2<sub>1</sub>/c* phase is small. To avoid correlation effects, the displacement parameters for the four equatorial oxygen atoms (O1, O2, O3, and O4) were constrained to be equal. However, even with this precaution, there was large uncertainty on the displacement and occupancy factors for O4 because of the low fraction of the *P2<sub>1</sub>/c* phase. To stabilize the refinements, geometric soft-restraints were used for the monoclinic phase from the beginning to the end of the

isotherm. For a good estimation of the standard deviations on interatomic distances for soft-restraints, the monoclinic structure at 500 °C was compared to that of the single *P2<sub>1</sub>/c* material at RT in the end of the experiment. The two-phase refinements carried out with these soft-restraints resulted in improved fits, as shown in Figure 5. For comparison purposes, a single-phase refinement of a pattern collected for 5 min after 50 min of heating at 500 °C resulted in  $\chi^2 = 6.06$  using *I4/mmm* while the two-phase refinement gives  $\chi^2 = 2.81$ .

After heating for 130 min at 500 °C, the tetragonal  $\rightarrow$  monoclinic phase transition was incomplete. The fraction of the monoclinic phase was  $\sim 24$  wt % and its composition



**Figure 8.** Observed and calculated diffraction patterns of  $\text{Sr}_2\text{MnO}_{4-\delta}$  after 80 min heating at  $550\text{ }^\circ\text{C}$ . The calculated diffraction pattern derives from a  $P2_1/c$  monoclinic model. The peaks clearly inconsistent with the tetragonal labeled (\*) are indexed as  $(-3\ 1\ 3)$ ,  $(2\ 3\ 1)$ ,  $(-1\ 3\ 4)$  at  $2\theta \sim 36.6^\circ$  and  $(-2\ 4\ 4)$ ,  $(0\ 4\ 4)$ ,  $(-3\ 1\ 5)$  at  $2\theta \sim 43.6^\circ$  in the  $P2_1/c$  space group.

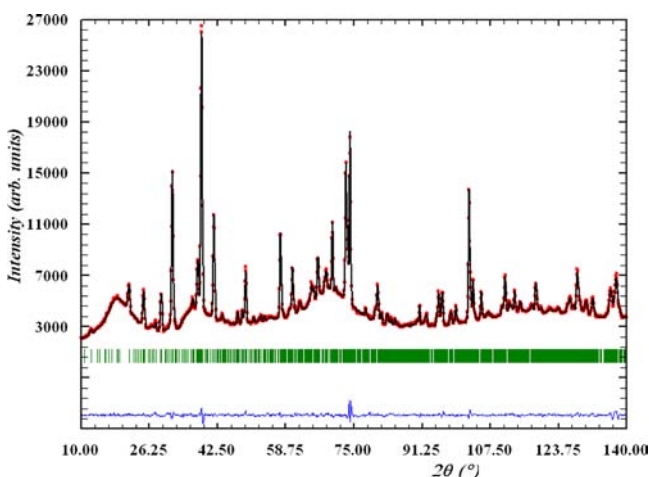


**Figure 9.** Observed and calculated diffraction patterns of  $\text{Sr}_2\text{MnO}_{3.55(1)}$  at  $RT$  after the second reducing cycle. The calculated diffraction pattern derives from a model consisting of a  $P2_1/c$  monoclinic phase. A difference profile is also shown.

$\text{Sr}_2\text{MnO}_{3.69(1)}$ . Oxygen loss continued on cooling, and the monoclinic fraction increased to  $\sim 41$  wt % at  $350\text{ }^\circ\text{C}$ . Between  $350\text{ }^\circ\text{C}$  and  $RT$ , the relative proportions of the tetragonal and monoclinic phases were constant. After the first reducing cycle, the NPD pattern collected at  $60\text{ }^\circ\text{C}$  revealed the presence of additional peaks (e.g., at  $2\theta \sim 101.4^\circ$ ) which were indexed in a monoclinic  $P2_1/c$  cell in agreement with that previously reported for the reduced Manganite  $\text{Sr}_2\text{MnO}_{3.64}$ .<sup>19</sup> Two-phase refinements based on  $I4/mmm$  and  $P2_1/c$  models gave an improved fit (Figure 6):  $\chi^2 = 2.71$ ,  $R_p = 8.25\%$ , and  $R_{wp} = 6.85\%$  (instead of  $\chi^2 = 7.91$ ,  $R_p = 14.1\%$ , and  $R_{wp} = 12.1\%$  for a single tetragonal phase) with the monoclinic phase being  $\sim 41$  wt %. The refined parameters, Table 2, indicate that the  $I4/mmm$  phase exhibits slight deficiency on the O2 position whereas a larger amount of oxygen vacancies occurs on the equatorial O4 site in the  $P2_1/c$  phase; the fractional occupancy 0.38 (4) on O4 results in the  $\text{Sr}_2\text{MnO}_{3.69(2)}$  stoichiometry.

To complete the reduction reaction, the sample was heated to  $550\text{ }^\circ\text{C}$  under hydrogen and isothermally held at  $550\text{ }^\circ\text{C}$  for 160 min. Two-phase sequential Rietveld refinements of the isothermal data carried out with the geometric soft-restraints outlined above, revealed that the phase-transition progresses and is complete after 80 min heating at  $550\text{ }^\circ\text{C}$ . Figure 7 highlights the progress of the reaction between  $440$  and  $550\text{ }^\circ\text{C}$  through the evolution of the intensity of two superstructure peaks.

Figure 8 shows a good single phase Rietveld refinement in  $P2_1/c$  of a pattern collected at  $550\text{ }^\circ\text{C}$ . The refined composition  $\text{Sr}_2\text{MnO}_{3.55(1)}$  remains unchanged on extended heating at  $550\text{ }^\circ\text{C}$  up to 160 min and subsequent cooling to  $RT$ .

The TECs of the monoclinic phase determined from the linear evolution of the lattice parameters on cooling from  $550\text{ }^\circ\text{C}$  are  $16.26 \times 10^{-6}\text{ K}^{-1}$  within the equatorial layers and  $11.14 \times 10^{-6}\text{ K}^{-1}$  along the perpendicular axis giving an average value of  $14.55 \times 10^{-6}\text{ K}^{-1}$ . The TEC in the equatorial layer is comparable to that of the tetragonal phase. For interpretation of the diffractograms collected at  $500$  and  $550\text{ }^\circ\text{C}$  in terms of kinetics of reduction, two methods were used. One was to monitor the evolution of the integrated intensity of a superstructure reflection (e.g., at  $36.6^\circ$ ) and the other method was based on least-squares refinements of the evolution of the weight fraction of the monoclinic phase. The kinetic constants obtained assuming single first order equations are similar irrespective of the method used; they are  $k_{500} = 0.110 \times 10^{-2}$  and  $k_{550} = 0.516 \times 10^{-2}\text{ min}^{-1}$  at  $500$  and  $550\text{ }^\circ\text{C}$ , respectively, indicating that both methods allow extracting kinetic information for the current reduction experiment. The activation energy for oxygen deintercalation from  $\text{Sr}_2\text{MnO}_{4-\delta}$  determined from an Arrhenius plot corresponds to  $E_a = 163\text{ kJ mol}^{-1}$ .

Rietveld refinements of the data collected at  $RT$  after the second reducing cycle gave a good fit using a single  $P2_1/c$  model which resulted in  $\chi^2 = 2.38$ ,  $R_{wp} = 6.63\%$ ,  $R_p = 7.64\%$ . The lattice parameters  $a = 6.85189(16)\text{ \AA}$ ,  $b = 10.80583(31)\text{ \AA}$ ,  $c = 10.81385(33)\text{ \AA}$ , and  $\beta = 113.291(3)^\circ$  are consistent with those determined from ex situ NPD of the reduced Manganite  $\text{Sr}_2\text{MnO}_{3.64}$ .<sup>19</sup> The Rietveld plot is displayed in Figure 9, and the refined parameters and Mn–O bond lengths are given in Tables 3 and 4, respectively.

#### 4. DISCUSSION

Previously, only tetragonal  $\text{Sr}_2\text{MnO}_4$  or monoclinic  $\text{Sr}_2\text{MnO}_{3.64}$  were observed at  $RT$  with no evidence for phase coexistence.<sup>19</sup> Moreover the symmetry of the reduced phase at high temperature was unknown. According to Gillie et al., the monoclinic  $P2_1/c$  symmetry is triggered by oxygen loss from the oxygen site O4, but the oxygen content below which the compound transits from tetragonal to monoclinic was unknown. To understand the reasons for the structural changes in the  $\text{Sr}_2\text{MnO}_{4-\delta}$  system, the evolution of the occupancy factor for O4 was monitored throughout the reducing cycles, as shown in Figure 10a. Five regions can be distinguished, displayed in Figure 10b:

1. On heating the as-prepared  $I4/mmm$   $\text{Sr}_2\text{MnO}_4$  material, the oxygen content and symmetry are unchanged up to  $T \sim 460\text{ }^\circ\text{C}$  and the evolution of the cell parameter reveals good thermo-mechanical compatibility with standard SOFC electrolytes.

Table 3. Structure Parameters of  $\text{Sr}_2\text{MnO}_{4-\delta}$  at 70 °C after the Second Reducing Cycle<sup>a</sup>

atom	x	y	z	$B_{\text{iso}}$ ( $\text{\AA}^2$ )	occupancy
Sr1	0.281(2)	-0.001(2)	0.072(2)	0.9(2)	1.0
Sr2	0.306(2)	0.000(2)	0.578(2)	0.4(3)	1.0
Sr3	0.292(3)	0.244(2)	0.335(2)	1.1(3)	1.0
Sr4	0.295(3)	0.746(1)	0.318(2)	0.4(2)	1.0
Mn1	-0.008(2)	0.002(2)	0.253(3)	0.33(5)*	1.0
Mn2	0.000(5)	0.255(3)	0.003(2)	0.33(4)*	1.0
O1	-0.006(2)	0.141(1)	0.127(1)	0.67(5)**	1.04(2)
O2	-0.002(3)	0.104(1)	0.395(2)	0.67(5)**	1.00(2)
O3	0.005(3)	0.128(1)	0.866(1)	0.67(5)**	0.98(3)
O4	0.01(2)	0.092(6)	0.571(9)	0.67(5)**	0.11(2)
O5	0.302(2)	-0.010(2)	0.335(2)	0.72(4)***	1.05(5)
O6	0.317(2)	0.013(2)	0.818(2)	0.72(4)***	1.04(5)
O7	0.311(3)	0.260(2)	0.091(2)	0.72(4)***	1.01(9)
O8	0.314(3)	0.741(2)	0.069(2)	0.72(4)***	1.01(9)

<sup>a</sup>Space group  $P2_1/c$ :  $a = 6.8517(2)$   $\text{\AA}$ ,  $b = 10.8063(3)$   $\text{\AA}$ ,  $c = 10.8134(3)$   $\text{\AA}$ ,  $\beta = 113.287(2)^\circ$ ,  $V = 735.41(36)$   $\text{\AA}^3$ ,  $Z = 8$ ,  $R_{\text{Bragg}} = 3.84\%$ ,  $R_{\text{wp}} = 6.63\%$ ,  $R_p = 7.64\%$ ,  $\chi^2 = 2.38$ . \*, \*\* and \*\*\* denote parameters constrained to be equal.

Table 4. Mn–O Bond Lengths ( $\text{\AA}$ ) from NPD Collected at 70 °C after the Second Reducing Cycle<sup>a</sup>

Mn1–O1	2.0175(1)	Mn2–O1	1.8438(1)
Mn1–O2	1.8694(1)	Mn2–O2	1.9072(1)
Mn1–O3	1.9156(1)	Mn2–O3	2.0409(1)
Mn1–O4	1.9454(1)	Mn2–O4	1.8115(1)
Mn1–O5	1.9652(3)	Mn2–O7	1.9703(3)
Mn1–O6	1.9459(3)	Mn2–O8	1.9720(1)

<sup>a</sup>For comparison, in  $\text{Sr}_2\text{MnO}_4$  (Table 1) the Mn–O1 and Mn–O2 bond lengths along the tetragonal axis and within the perovskite layers are 1.950(1)  $\text{\AA}$  and 1.89463(1)  $\text{\AA}$ , respectively.

- Oxygen loss starts above  $T \sim 460$  °C and goes faster with the increase in temperature and continues on isothermal heating at 500 °C and cooling to 350 °C. Comparison of Figures 10a and 10b shows that the onset of the tetragonal  $\rightarrow$  monoclinic phase transition occurs at the stoichiometry  $\text{Sr}_2\text{MnO}_{3.69(2)}$  reached at 500 °C in our heating conditions (heating rate, 5%  $\text{H}_2$  dilution and flow rate 3.6  $\text{L h}^{-1}$ ). The oxygen composition of both the tetragonal and the monoclinic phases vary on isothermal heating at 500 °C and cooling; at the same time the

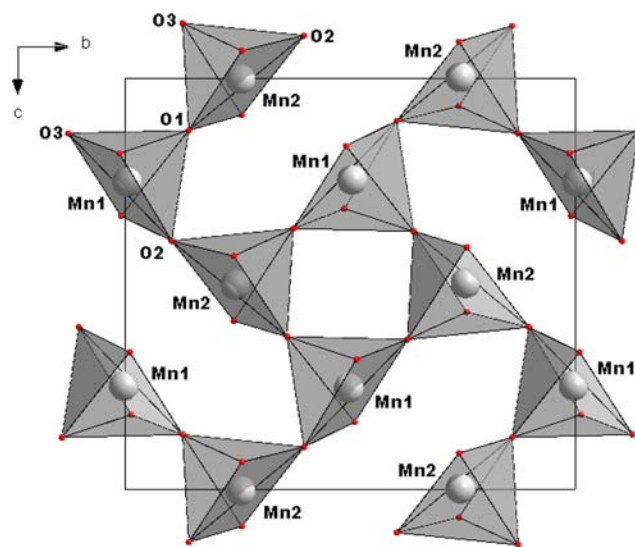


Figure 11. Ordered oxygen defects perovskite layer of  $\text{Sr}_2\text{MnO}_{3.55}$  within the  $bc$  plane in the monoclinic lattice derived from the Rietveld refinement at RT. The O4 position/atom is not included as it is only  $\sim 11\%$  occupied.

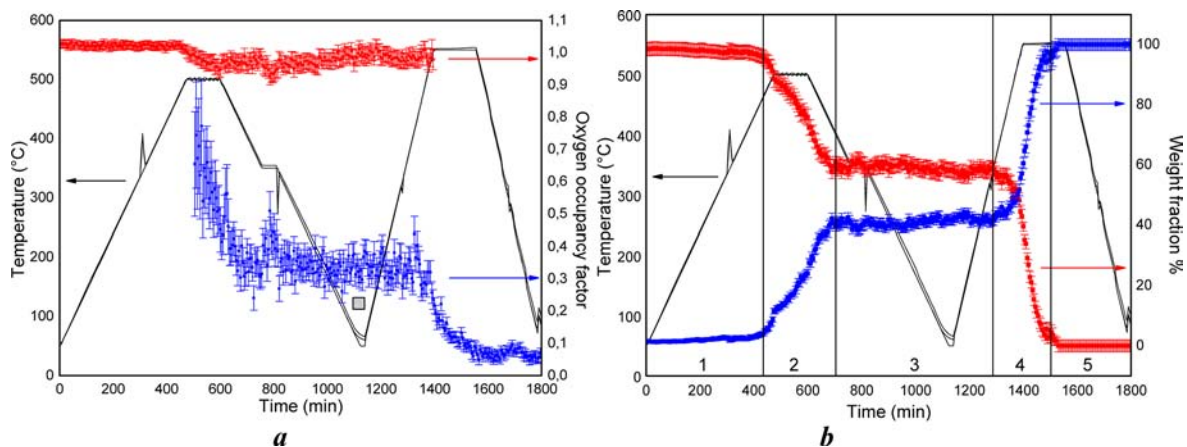


Figure 10. Evolution of the (a) oxygen occupancy factor of the (red) O2 site in the tetragonal phase and (blue) O4 site in the  $P2_1/c$  phase throughout the reducing cycles under 5%  $\text{H}_2$ -He and, (b) weight fraction of (red)  $I4/mmm$   $\text{Sr}_2\text{MnO}_4$  and (blue)  $P2_1/c$   $\text{Sr}_2\text{MnO}_{4-\delta}$ . The oxygen occupancy obtained by Gillie et al.<sup>19</sup> is indicated by a square in (a).

fraction of the monoclinic phase increases up to ~24 wt % after 150 min heating at 500 °C and keeps growing on cooling, to reach ~41 wt % at 350 °C.

- Below 350 °C, the weight fractions and oxygen compositions of the tetragonal and monoclinic phases are unchanged.
- On heating above 350 °C up to 550 °C, the oxygen occupancy of O4 decreases along with increase in the fraction of the monoclinic phase. At 550 °C, the proportion of the *I4/mmm* is very small and only its scale factor is refined while the structural and profile parameters were fixed at the values obtained at the beginning of the isotherm.
- Finally, after 80 min of heating at 550 °C, the tetragonal phase has completely transformed into a monoclinic phase whose composition refined to Sr<sub>2</sub>MnO<sub>3.55(1)</sub>. No change in composition or symmetry is observed on extended isothermal heating and subsequent cooling to RT. The Sr<sub>2</sub>MnO<sub>3.55(1)</sub> composition is most likely the stable phase with the lowest well-defined oxygen content.

The *I4/mmm* Sr<sub>2</sub>MnO<sub>4.00</sub> → *P2<sub>1</sub>/c* Sr<sub>2</sub>MnO<sub>3.55(1)</sub> phase transition is associated to a molar volume expansion of 2.44% (Tables 1 and 3). These Sr<sub>2</sub>MnO<sub>3.69(2)</sub> → *I4/mmm* Sr<sub>2</sub>MnO<sub>4.00</sub> and Sr<sub>2</sub>MnO<sub>3.55(1)</sub> Sr<sub>2</sub>MnO<sub>4.00</sub> are reversible according to Kriegel et al.<sup>21</sup> and Munnings et al., respectively.<sup>39</sup> Munnings et al. found by in situ NPD in air that oxidation of Sr<sub>2</sub>MnO<sub>3.5+x</sub> proceeds at ~275 °C with a change from monoclinic to tetragonal symmetry.<sup>39</sup> Our moderate reduction conditions and neutron diffraction data indicate narrow structural relations between the *I4/mmm* and *P2<sub>1</sub>/c* phases consistent with simple relations between the lattice constants  $a_m = 1/2 (-a_t - b_t + c_t)$ ,  $b_m = 2 (-a_t + b_t)$ ,  $c_m = 2 (a_t + b_t)$ . Gillie et al.<sup>19</sup> reported that the reduction is topotactic. Only the octahedral coordination of Mn (IV) is decreased to a square pyramidal environment around Mn (III) with concomitant reduction in crystal symmetry. The structure of Sr<sub>2</sub>MnO<sub>3.55(1)</sub> consists in two-dimensional linkage of corner-sharing MnO<sub>5</sub> pyramids derived by removing equatorial oxygen from the “MnO<sub>2</sub>” layers of Sr<sub>2</sub>MnO<sub>4</sub>.<sup>19</sup> The oxygen shared by two neighboring pyramids belongs, in one case, to the basal planes of both pyramids and in another case to the basal plane of one pyramid and the apex of another one. An anion vacancy produces two Mn (III) ions in the basic faces of square pyramids facing each other, as illustrated in Figure 11. The slight occupancy of the O4 site (Table 3) affects the bond lengths; two of them Mn1–O1 and Mn2–O3 are particularly long (Table 4). Indeed, the top of the square-based pyramids centered on Mn1 and Mn2 are respectively O1 and O3, and the O4 site is between these basal planes. Therefore, the repulsion between Mn1 and Mn2 and consequent lengthening the Mn1–O1 and Mn2–O2 bonds might be the driving force for the volume expansion of Sr<sub>2</sub>MnO<sub>3.55(1)</sub> and symmetry reduction.

The oxygen stoichiometries refined for the single phase as-prepared and reduced materials are consistent with the weight loss obtained from TGA. The kinetics constants for the reduction reaction determined from the sequential refinements of the NPD patterns collected during isothermal heating at 500 and 550 °C are  $k_{500} = 0.110 \times 10^{-2}$  and  $k_{550} = 0.516 \times 10^{-2} \text{ min}^{-1}$ , respectively. It should be borne out that heterogeneous reactions depend upon the particle size of the solid and difference in specific surface areas affect the rates for the oxygen exchange processes. The activation energy for oxygen

deintercalation is  $E_a = 163 \text{ kJ mol}^{-1}$ . Since there is no kinetic data for the reduction of manganites, this  $E_a$  value can be compared with the activation energy data available for the oxidation of La<sub>1-x</sub>Sr<sub>x</sub>MnO<sub>3.0</sub> (LSM) in air (136–160 kJ mol<sup>-1</sup>) determined from in situ synchrotron powder diffraction studies.<sup>40</sup> However our Arrhenius plot consists of only two kinetic values, at 500 and 550 °C, and therefore gives no evidence that only one rate-determining step is involved in the reduction process of Sr<sub>2</sub>MnO<sub>4-δ</sub> as demonstrated for the oxidation of LSM.<sup>40</sup>

## 5. CONCLUSIONS

Time-resolved NPD is a versatile tool for the in situ investigation of solid/gas chemical reactions. The results presented in this paper have shown that not only structural but also thermodynamic and kinetic information of reaction and phase transitions can be obtained through in situ time-resolved powder diffraction. As discussed above the tetragonal Sr<sub>2</sub>MnO<sub>4</sub> material heated under dilute hydrogen flow loses oxygen from the “MnO<sub>2</sub>” equatorial layer above  $T \sim 470 \text{ °C}$  with retention of tetragonal symmetry up to Sr<sub>2</sub>MnO<sub>3.70(1)</sub>. Further oxygen loss induces ordering of the oxygen vacancies within the equatorial layers transforming the tetragonal cell into a *P2<sub>1</sub>/c* monoclinic supercell. When the phase transition is complete, the composition of the single-phase *P2<sub>1</sub>/c* material refined to Sr<sub>2</sub>MnO<sub>3.55(1)</sub> and does not vary on extended heating. Comparison with the Sr<sub>2</sub>MnO<sub>3.64</sub> material obtained from ex situ heat treatment at 550 °C under 10% H<sub>2</sub>–N<sub>2</sub> at 550 °C reveals that in situ reduction allows reaching a higher degree of reduction with almost single Mn<sup>3+</sup> oxidation state although the pure Mn<sup>3+</sup> material Sr<sub>2</sub>MnO<sub>3.50</sub> could not be obtained. It is interesting to emphasize that the structure of Sr<sub>2</sub>MnO<sub>3.55(1)</sub> at high temperature is monoclinic and does not vary with the cooling rate and is therefore consistent with the RT symmetry determined for the Sr<sub>2</sub>MnO<sub>3.64</sub> reduced material.<sup>19</sup> The decomposition of Sr<sub>2</sub>MnO<sub>4</sub> at  $T \geq \sim 600 \text{ °C}$  under hydrogen atmosphere and the first-order reversible phase transition occurring below 550 °C and the associated great volume change (2.44%) linked to the reduction of Mn<sup>4+</sup> to the Jahn–Teller Mn<sup>3+</sup> ion prevent application of Sr<sub>2</sub>MnO<sub>3.55(1)</sub> as anode material for SOFC.

## AUTHOR INFORMATION

### Corresponding Author

\*E-mail: mona.bahout@univ-rennes1.fr (M.B.); c.greaves@bham.ac.uk (C.G.). Tel: +44-121-4144397 (C.G.).

### Notes

The authors declare no competing financial interest.

## ACKNOWLEDGMENTS

We thank A. Daramsy for assistance with the collection of the NPD data at ILL. One of the authors (M.B.) thanks P. D. Battle for discussion and help.

## REFERENCES

- Tokura, Y. *Colossal Magnetoresistive Oxides*; Breach Science Publishers: New York, 1999.
- Moritomo, Y.; Asamitsu, A.; Kuwahara, H.; Tokura, Y. *Nature* **1996**, *380*, 141–144.
- Battle, P. D.; Blundell, S. J.; Green, M. A.; Hayes, W.; Honold, M.; Klehe, A. K.; Laskey, N. S.; Millburn, J. E.; Murphy, L.; Rosseinsky, M. J.; Samarin, N. A.; Singleton, J.; Sluchanko, N. E.; Sullivan, S. P.; Vente, J. F. *J. Phys.: Condens. Matter* **1996**, *8*, L427–L434.

- (4) Battle, P. D.; Green, M. A.; Laskey, N. S.; Millburn, J. E.; Radaelli, P. G.; Rosseinsky, M. J.; Sullivan, S. P.; Vente, J. F. *Phys. Rev. B* **1996**, *54*, 15967.
- (5) Minh, N. Q. *J. Am. Ceram. Soc.* **1993**, *76*, 563–588.
- (6) Amow, G.; Skinner, S. J. *Solid State Electrochem.* **2006**, *10*, 538–546.
- (7) Caneiro, A.; Moggi, L.; Grunbaum, N.; Prado, F. J. *Therm. Anal. Calorim.* **2011**, *103*, 597–606.
- (8) Skinner, S.; Kilner, J. *Ionics* **1999**, *5*, 171–174.
- (9) Kilner, J. A.; Shaw, C. K. M. *Solid State Ionics* **2002**, *154*–155, 523–527.
- (10) Mauvy, F.; Bassat, J. M.; Boehm, E.; Dordor, P.; Grenier, J. C.; Loup, J. P. *J. Eur. Ceram. Soc.* **2004**, *24*, 1265–1269.
- (11) Skinner, S. J.; Kilner, J. A. *Solid State Ionics* **2000**, *135*, 709–712.
- (12) Bassat, J. M.; Odier, P.; Villesuzanne, A.; Marin, C.; Pouchard, M. *Solid State Ionics* **2004**, *167*, 341–347.
- (13) Munnings, C. N.; Skinner, S. J.; Amow, G.; Whitfield, P. S.; Davidson, I. J. *Solid State Ionics* **2006**, *177*, 1849–1853.
- (14) Sun, L. P.; Huo, L. H.; Zhao, H.; Li, Q.; Pijolat, C. J. *Power Sources* **2008**, *179*, 96–100.
- (15) Benabad, A.; Daoudi, A.; Salmon, R.; Le Flem, G. J. *Solid State Chem.* **1977**, *22*, 121–126.
- (16) Jean-Claude Bouloux, J.-L. S.; Le Flem, G.; Hagen-guller, P. J. *Solid State Chem.* **1981**, *38*, 34–39.
- (17) Mizutani, N.; Ohkuma, N.; Kitazawa, A.; Kato, M. *Kog Kagaku Zasshi* **1970**, *73*, 1103–8.
- (18) Balz, D.; Pleith, K. Z. *Elektrochem.* **1955**, *59*, 545.
- (19) Gillie, L. J.; Wright, A. J.; Hadermann, J.; Van Tendeloo, G.; Greaves, C. J. *Solid State Chem.* **2002**, *167*, 145–151.
- (20) Kriegel, R.; Borrmann, H.; Simon, A.; Feltz, A. Z. *Naturforsch., B: Chem. Sci.* **1993**, *48*, 15–18.
- (21) Kriegel, R.; Preu, N.; gb. *Thermochim. Acta* **1996**, *285*, 91–98.
- (22) Caignaert, V.; Nguyen, N.; Hervieu, M.; Raveau, B. *Mater. Res. Bull.* **1985**, *20*, 479–484.
- (23) Caignaert, V. *J. Magn. Magn. Mater.* **1997**, *166*, 117–123.
- (24) Nakamura, T.; Petzow, G.; Gauckler, L. J. *Mater. Res. Bull.* **1979**, *14*, 649–659.
- (25) Al Daroukh, M.; Vashook, V. V.; Ullmann, H.; Tietz, F.; Arual Raj, I. *Solid State Ionics* **2003**, *158*, 141–150.
- (26) Li, R. K.; Greaves, C. J. *Solid State Chem.* **2000**, *153*, 34–40.
- (27) Mitchell, J. F.; Millburn, J. E.; Medarde, M.; Short, S.; Jorgensen, J. D.; Fernández-Díaz, M. T. *J. Solid State Chem.* **1998**, *141*, 599–603.
- (28) Poepplmeier, K. R.; Leonowicz, M. E.; Scanlon, J. C.; Longo, J. M.; Yelon, W. B. *J. Solid State Chem.* **1982**, *45*, 71–79.
- (29) Leonowicz, M. E.; Poepplmeier, K. R.; Longo, J. M. *J. Solid State Chem.* **1985**, *59*, 71–80.
- (30) T. C. Hansen, P. F. H.; Fischer, H. E.; Torregrossa, J.; Convert, P. *Meas. Sci. Technol.* **2008**, *19*, 034001.
- (31) Tonus, F.; Bahout, M.; Battle, P. D.; Hansen, T.; Henry, P. F.; Roisnel, T. *J. Mater. Chem.* **2010**, *20*, 4103–4115.
- (32) Rietveld, H. J. *Appl. Crystallogr.* **1969**, *2*, 65–71.
- (33) L. B. McCusker, R. B. V. D.; Cox, D. E.; Louer, D.; Scardie, P. J. *Appl. Crystallogr.* **1999**, *32*, 36–50.
- (34) Rodríguez-Carvajal, J. *Phys. B* **1993**, *192*, 55–69.
- (35) Petricek, V.; Dusek, M., 2000.
- (36) Berar, J.-F.; Baldinozzi, G. *J. Appl. Crystallogr.* **1993**, *26*, 128–129.
- (37) Kharton, V. V.; Marques, F. M. B.; Atkinson, A. *Solid State Ionics* **2004**, *174*, 135–149.
- (38) Kharton, V. V.; Tsipis, E. V.; Marozau, I. P.; Viskup, A. P.; Frade, J. R.; Irvine, J. T. S. *Solid State Ionics* **2007**, *178*, 101–113.
- (39) Munnings, C. N.; Sayers, R.; Stuart, P. A.; Skinner, S. J. *Solid State Sci.* **2012**, *14*, 48–53.
- (40) Krogh Andersen, E.; Krogh Andersen, I. G.; Norby, P.; Hanson, J. C. *J. Solid State Chem.* **1998**, *141*, 235–240.